Pergamon

Int. J. Solids Structures Vol. 32, No. 3/4, pp. 341–355, 1995

0020–7683/95 $9.50 + .00

0020–7683(94)00125–1

FAILURE MECHANISMS AND DAMAGE EVOLUTION IN CROSSPLY CERAMIC-MATRIX COMPOSITES

I. M. DANIEL and G. ANASTASSOPOULOS
McCormick School of Engineering and Applied Science, Northwestern University, Evanston, IL 60208, U.S.A.

(*Received* 17 *June* 1994)

Abstract—Failure mechanisms were studied under the microscope in a crossply silicon carbide/glass-ceramic composite under axial tensile loading. Failure initiation takes place in the 90° layer. It takes the form of radial matrix cracks around the fibers, followed by interfacial cracks, which in turn coalesce into transverse macrocracks. These transverse macrocracks in the 90° layer reach a characteristic saturation crack density with a minimum crack spacing of the order of the layer thickness. Subsequently, transverse matrix cracks are generated in the 0° layer, increasing in density up to a minimum crack spacing of the order of eight fiber diameters. This stage of failure is accompanied by fiber–matrix debonding and some fiber-failures in the 0° layer. In the third stage of damage development, the macrocracks of the 90° layer branch off and connect with the 0° layer cracks in a characteristic "delta" pattern. This is finally followed by delamination and additional cracking in the 90° layer prior to ultimate failure. The various failure mechanisms and their interactions were discussed and compared with predictions of prior experimental and analytical studies of unidirectional and crossply composites.

1. INTRODUCTION

The newer generation of advanced composites designed to meet high temperature performance requirements includes ceramic-matrix composites. Ceramic composites display appreciable ductility and have higher fracture toughness and better fatigue endurance than comparable monolithic ceramics. Promising reinforcements include carbon, silicon carbide (SiC) and mullite fibers. Matrices used successfully include glass, glass-ceramic, carbon, silicon carbide, silicon nitride and aluminum oxide. Composites consisting of glass-ceramic matrices, such as lithium aluminosilicate (LAS), calcium aluminosilicate (CAS) and magnesium aluminosilicate (MAS) reinforced with silicon carbide yarn or monofilament have been developed; see Prewo and Brennan (1982), Brennan and Prewo (1982), Larsen and Adams (1989). These materials can be fabricated in both unidirectional and multidirectional laminate form, and can attain strengths of 1000 MPa (140 ksi) and ultimate strains of over 1%. Fracture toughness, as determined by a notched beam method, is more than five times that of the monolithic ceramic, Brennan and Prewo (1982).

The micromechanics of stress transfer and fracture have been studied experimentally and analytically by many investigators for the case of unidirectional composites, starting with the pioneering work by Aveston *et al.* (1971) and Aveston and Kelly (1973). Fundamental approaches used include shear lag or stress transfer models and fracture mechanics with stress or energy fracture criteria. Failure mechanisms in a SiC/LAS unidirectional composite under longitudinal loading have been observed and analyzed by Marshall and Evans (1985, 1988) and Marshall *et al.* (1985). Further analytical studies were described by Budiansky et al. (1986), Hsueh (1988), Charalambides and Evans (1989), McCartney (1989), Hutchinson and Jenson (1990), Zok and Spearing (1992) and Weitsman and Zhu (1993). The authors have reported both experimental and analytical investigations of a longitudinally and transversely loaded unidirectional SiC/CAS composite; see Daniel *et al.* (1989a,b, 1992, 1993) and Lee and Daniel (1992). Most studies to date on the behavior of composites under transverse loading are analytical, such as those by Hashin (1983), Benveniste (1985) and Achenbach and Zhu (1990).

The problem of crossply laminates has been studied extensively for polymer-matrix composites. The primary failure mechanism in these composites is transverse matrix cracking in the 90° layer reaching a limiting crack density. This is followed by longitudinal matrix cracking in the 0° layers, local delaminations at the intersections of matrix cracks and, finally, fiber fractures in the 0° layer leading to ultimate failure, Daniel *et al.* (1988). In the case of brittle-matrix composites the type, sequence and interaction of failure mechanisms are different and characteristic of the constituent material properties. Some experimental work on crossply ceramic-matrix composites has been reported by Sbaizero and Evans (1986). They tested symmetric $[0/90]_s$ SiC/LAS laminates in tension and bending. However, the observed failure modes were not easily explained. The initial delamination failure observed would only be possible near free edges in the case of a material with very low interlaminar shear strength. The orientation of the transverse ply cracks could only be explained by assuming compressive residual stresses in the 90° layers. Subsequent work on crossply laminates dealt with a fracture mechanics model of a delamination crack formed at the tip of a notch cutting through 0° and 90° layers, see Sbaizero *et al.* (1990) and Charalambides (1991). Mall and Kim (1992) also conducted experimental investigations of failure mechanisms in SiC/CAS laminates. They observed that initial failure consisted of matrix microcracks occurring and growing in all plies in a random manner.

This paper deals with a systematic investigation of the failure mechanisms, their growth and interactions in a crossply SiC/CAS laminate under uniaxial tension. It represents the first systematic experimental/analytical study of a crossply laminate with brittle matrix. Previous experimental work mentioned before reported random or other edge-dominated failure mechanisms with no clear trends. The failure mechanisms observed and recorded in the present study are substantially different from those reported before and show a clear and systematic trend. The initial stages of failure in each layer are interpreted on the basis of the failure micromechanics of the unidirectional material under longitudinal and transverse loading. The interaction of failure mechanisms in the 0° and 90° layers and the later stages of damage are explained on the basis of classical lamination theory as well as on damage models available for crossply laminates. The various failure mechanisms and damage states were correlated with the overall mechanical behavior of the laminate. The main contribution of this paper lies in the integration of the micromechanics of brittle matrix single layers and the macromechanics of a crossply laminate in predicting and interpreting the type and sequence of failure mechanisms and their interaction.

2. EXPERIMENTAL PROCEDURE

The material investigated was SiC/CAS, calcium aluminosilicate glass-ceramic reinforced with silicon carbide fibers, manufactured by Corning Glass Works. The fiber is silicon carbide yarn known as Nicalon (Nippon Carbon Co.). This fiber is available in continuous length tows with an average diameter of 15 μm. The composite material for this study was obtained in the form of unidirectional and $[0/90]_{2s}$ and $[0/90_2]_s$ crossply laminates.

The unidirectional material was characterized first to obtain average physical and mechanical properties. Unidirectional specimens instrumented with strain gages were tested under longitudinal and transverse tensile loading in a servohydraulic testing machine.

The macroscopic response of the crossply laminates was measured by testing specimens under axial tension. The specimens were 15.2 cm (6 in.) long and 1.27 cm (0.5 in.) wide. They were tabbed with 3.81 cm (1.5 in.) long crossply glass/epoxy tabs. These specimens were tested in a servohydraulic testing machine (Instron) using an extensometer to monitor strain to failure.

Failure mechanisms were monitored by testing smaller crossply coupons under the microscope with a specially designed fixture. The specimens were 76 mm (3 in.) long and 12.7 mm (0.5 in.) wide coupons. Potting epoxy was cast around these coupons to help in subsequent polishing and loading of the specimen. One edge of the specimen was polished for microscopic observations.

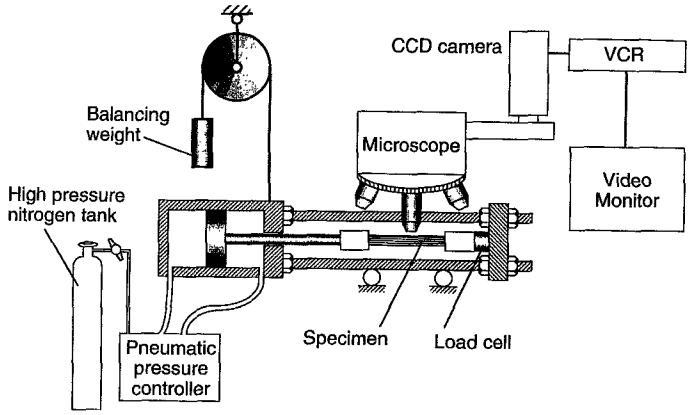

Fig. 1. Setup for microscopic observation of failure mechanisms in composite specimens under load.

A special loading fixture was designed and built for loading the specimens under the microscope (Fig. 1); see Daniel *et al.* (1989a,b). Load was applied and controlled by means of a pneumatic cylinder. The specimen with the grips attached was mounted onto a reaction frame attached to one end of the pneumatic cylinder. One end of the specimen was connected to the moving piston while the other end was reacted at the other end of the reaction frame through a strain gage load cell. The entire assembly, including air cylinder, reaction frame, specimen with grips and load cell, was suspended with a counterweight from a movable upright frame. Thus, any part of the loaded specimen could be moved to the stage of the microscope without any weight or force exerted on the microscope.

Two types of tests were conducted, continuous and intermittent loading tests. In the first type, loading is applied continuously to failure. A specific area of the specimen is observed through the microscope and recorded by a video camera. This type of loading yields a continuous stress–strain curve not affected by stress relaxation, as is the case during intermittent loading. However, only one small area of the specimen is being monitored and many interesting phenomena occurring outside the field of view are missed.

In the second type of test, loading is applied in steps. The stress and strain in the specimen are recorded in the beginning and at the end of each loading step. Photomicrographs are taken at different areas of the specimen while the strain is held constant. One problem in this type of testing is stress relaxation during the holding period, which becomes more pronounced as damage progresses.

3. RESULTS

Material characterization

Some basic properties of the matrix and fiber constituents obtained from the literature and from previous tests are tabulated in Table 1.

Table 1. Constituent material properties

Property	CAS matrix†	SiC fiber‡
Maximum use temperature, °C (°F)	1350 (2460)	1300 (2370)
Fiber diameter (μm)	—	15
Density (g cm^{-3})	2.8	2.6
Coefficient of thermal expansion, 10^{-6}°C^{-1} (10^{-6}°F^{-1})	5.0 (2.8)	3.2 (1.8)–4.9 (2.7)
Elastic modulus, GPa (10^6 psi)	98 (14.2)	170 (24.6)
Tensile strength, MPa (ksi)	124 (18) (flexural)	1930 (280)

† Larsen and Adams (1989).
‡ Prewo and Brennan (1982), Daniel *et al.* (1989).

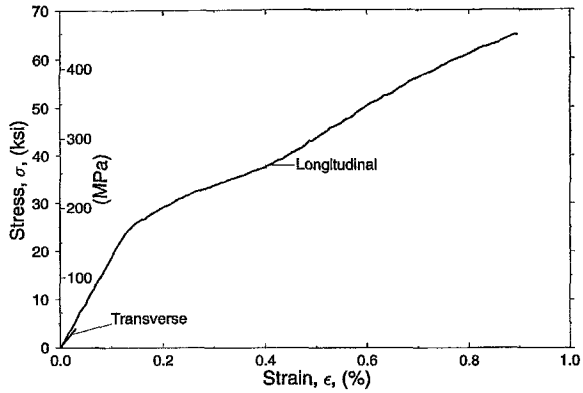

Fig. 2. Stress–strain curves to failure of unidirectional SiC/CAS composite under longitudinal and transverse tension.

Examination of photomicrographs of transverse cross-sections showed that the fiber diameter ranges between 8 and 20 μm, with a median value of 15 μm. The fiber distribution is nonuniform with an average fiber volume ratio of $V_f = 0.39$. A low degree of porosity was measured ($V_v = 0.01$).

Typical stress–strain curves to failure of the unidirectional composite under longitudinal and transverse tension are shown in Fig. 2. Basic properties obtained from such macromechanical tests of the unidirectional SiC/CAS composite are tabulated in Table 2.

Damage initiation and development in 90° *layer*

The first stage of damage development, consisting of microcracking in the 90° layers, was studied by testing $[0/90]_{2s}$ crossply laminates under the microscope; see Daniel *et al.* (1989a,b). The first microcracks originated at the fiber–matrix interface and were nearly normal to the interface, which indicates that failure is caused by the circumferential tensile stress in the matrix. The randomness of the fiber packing makes it difficult to draw conclusions. However, some general patterns can be identified.

When the fibers are closely packed, usually in a near hexagonal array, radial cracks initiate at approximately 45° from the loading axis. An analysis for a closely packed hexagonal array of fibers showed that for a low stiffness interphase, the peak circumferential stress is the critical one and it occurs near the 45° location, Achenbach and Zhu (1990). This of course leads to radial cracking at this location, as observed experimentally.

When fibers are farther apart and are surrounded by a relatively large volume of matrix, radial cracks occur at approximately 90° from the loading axis. For a low stiffness

Table 2. Measured properties of SiC/CAS unidirectional composite

Property	Value
Fiber volume ratio, V_f	0.39
Ply thickness, t, mm (in.)	0.38 (0.015)
Longitudinal modulus, E_1, GPa (Msi)	127 (18.4)
Transverse modulus, E_2, GPa (Msi)	112 (16.2)
In-plane shear modulus, G_{12}, GPa (Msi)	52 (7.5)
Out-of-plane shear modulus, G_{23}, GPa (Msi)	32 (4.7)
Major Poisson's ratio, ν_{12}	0.18
Longitudinal tensile strength, F_{1t}, MPa (ksi)	448 (65)
Transverse tensile strength, F_{2t}, MPa (ksi)	28 (4)
Longitudinal ultimate tensile strain, ε^u_{1t}	9×10^{-3}
Transverse ultimate tensile strain, ε^u_{2t}	2.5×10^{-4}
Longitudinal coefficient of thermal expansion, α_1, $\mu\varepsilon°K^{-1}$ ($\mu\varepsilon°F^{-1}$)	4.05 (2.25)
Transverse coefficient of thermal expansion, α_2, $\mu\varepsilon°K^{-1}$ ($\mu\varepsilon°F^{-1}$)	4.23 (2.35)
Out-of-plane coefficient of thermal expansion, α_3, $\mu\varepsilon°K^{-1}$ ($\mu\varepsilon°F^{-1}$)	4.32 (2.40)

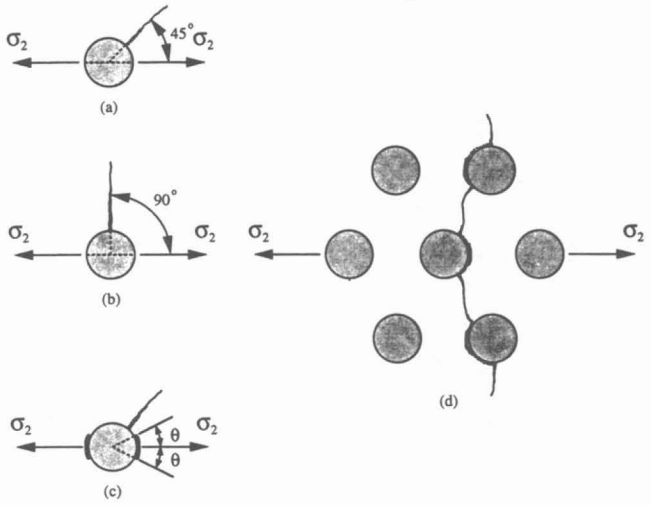

Fig. 3. Development of failure mechanisms in transversely loaded ceramic matrix composite. (a) Initial radial cracks around closely-packed fibers. (b) Initial radial cracks around isolated fibers. (c) Interfacial cracks. (d) Interconnection of radial and interfacial cracks and formation of macrocracks.

interphase the circumferential stress at the 90° location becomes critical, resulting in the observed radial cracks, Daniel *et al.* (1989).

As the load increases, a new failure mechanism develops, consisting of interface cracks in the area along the loading axis over an arc 2θ about the 0° point with $\theta < 45°$. These interface cracks are not immediately connected with the radial cracks developed earlier. Additional radial cracks may develop at this stage of damage development, and then, radial and interfacial cracks are connected to form a long continuous crack in the transverse layer. The various failure mechanisms and their sequence are illustrated schematically in Fig. 3.

The influence of these failure mechanisms on the stress–strain behavior of the $[0/90]_{2s}$ crossply laminate is shown in Fig. 4. The laminate behaves linearly up to an applied stress of 27.6 MPa (4 ksi) when the first radial cracks appear in the matrix. This causes a sudden drop in stiffness (secant modulus). At a higher applied stress, 32.4 MPa (4.7 ksi), interfacial cracking occurs causing another sudden, but smaller drop in stiffness. The interconnection of radial and interfacial cracks starts at a higher stress (36.6 MPa; 5.3 ksi) and progresses more gradually to the formation of continuous macrocracks, resulting in similarly gradual reduction in laminate stiffness. Similar stiffness reductions have been predicted by Zhu and Achenbach (1991) for a transversely loaded composite of the same properties, undergoing the same failure process.

The stiffness reductions illustrated in Fig. 4 are more pronounced in this test due to creep effects. The loading was applied intermittently over a relatively long period (more

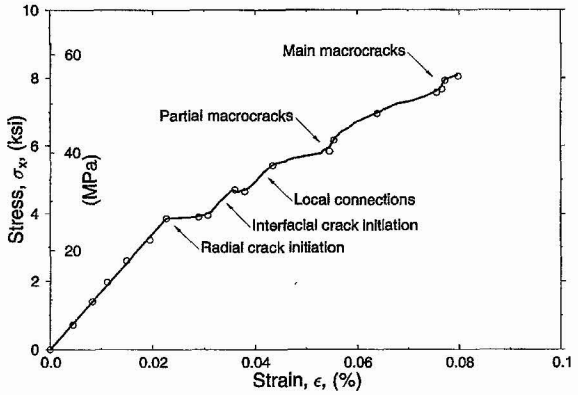

Fig. 4. Stress–strain curve of $[0/90]_{2s}$ crossply laminate with corresponding stages of damage development in transverse layer.

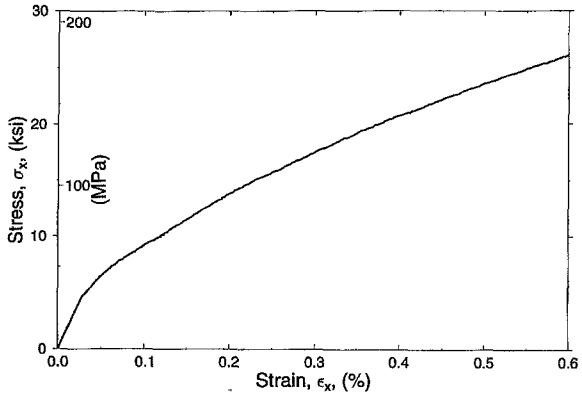

Fig. 5. Stress–strain curve of $[0/90_2]_s$ SiC/CAS crossply laminate under uniaxial tension.

than 30 min) to allow for photomicrographic recording of the various stages of damage development. The first continuous (across the 90° layer) macrocracks were formed at an applied stress of approximately 40 MPa (5.8 ksi), which corresponds to an axial stress of $\sigma_2 = 38$ MPa (5.5 ksi) in the 90° layer. The *in situ* lamina strength is comparable to the value measured by Mall and Kim (1992) and is higher than the transverse tensile strength $F_{2t} = 28$ (4 ksi) measured from a 90° transverse tensile test. Continued loading increases the number of macrocracks up to a saturation density, corresponding to a minimum macrocrack spacing of the order of the 90° layer thickness.

Figure 5 shows a stress–strain curve for a $[0/90_2]_s$ crossply laminate under uniaxial tension. Microcracking in the 90° layer (layer 2) started at an applied strain of approximately 0.025%. Transverse macrocracks reached a minimum crack spacing of 0.65 mm (0.0255 in.), comparable to the layer thickness of 0.68 mm (0.027 in.), at an applied stress of approximately 69 MPa (10 ksi), corresponding to a strain of approximately 0.12%.

The initial modulus in the linear region is

$$\bar{E}_x = 117\,\text{GPa}\,(16.9\,\text{Msi}),$$

which agrees with the calculated laminate modulus. The reduced secant modulus at the point of crack saturation ($\bar{\sigma}_x = 69$ MPa, $\bar{\varepsilon}_x = 0.12\%$) is

$$\bar{E}'_x = 58\,\text{GPa}\,(8.3\,\text{Msi}).$$

At this stage of damage development, corresponding to the proportional limit of the stress–strain response of the 0° layer (Fig. 2), no appreciable damage has occurred in the 0° layer (layer 1). Simple lamination analysis gives the following axial moduli and average axial stresses in the two layers:

$$E_1 = 127\,\text{GPa}\,(18.4\,\text{Msi})$$
$$E'_2 = 22.8\,\text{GPa}\,(3.3\,\text{Msi})$$
$$\sigma_{1x} = 152\,\text{MPa}\,(22\,\text{ksi})$$
$$\sigma_{2x} = 27.6\,\text{MPa}\,(4.0\,\text{ksi}),$$

where E_1 = initial modulus of 0° layer, E'_2 = degraded modulus of 90° layer, σ_{1x}, σ_{2x} = average axial (x-direction) stresses in layers 1 and 2, respectively.

Damage initiation and development in 0° layer

Prior investigations have shown that, in a unidirectional SiC/CAS composite under longitudinal tension, transverse matrix cracking starts at an applied strain of approximately 0.1%, see Daniel *et al.* (1993). This value is slightly below the proportional limit of the

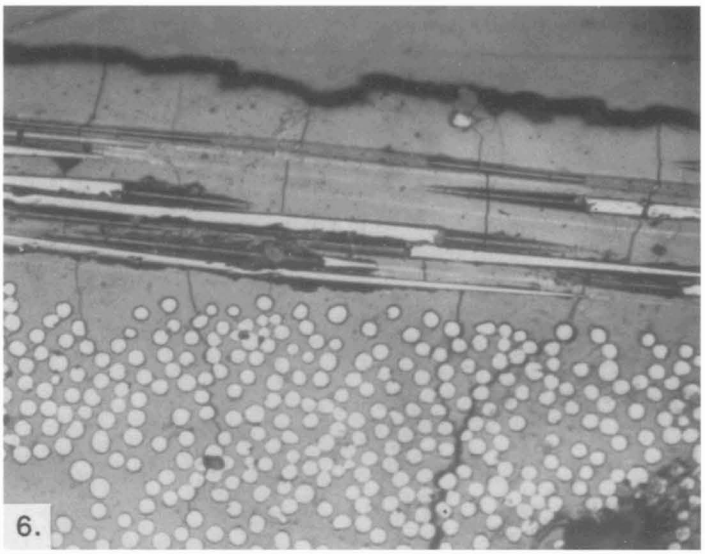

Fig. 6. Matrix cracking in 0°-ply following saturation of cracking in 90°-ply.

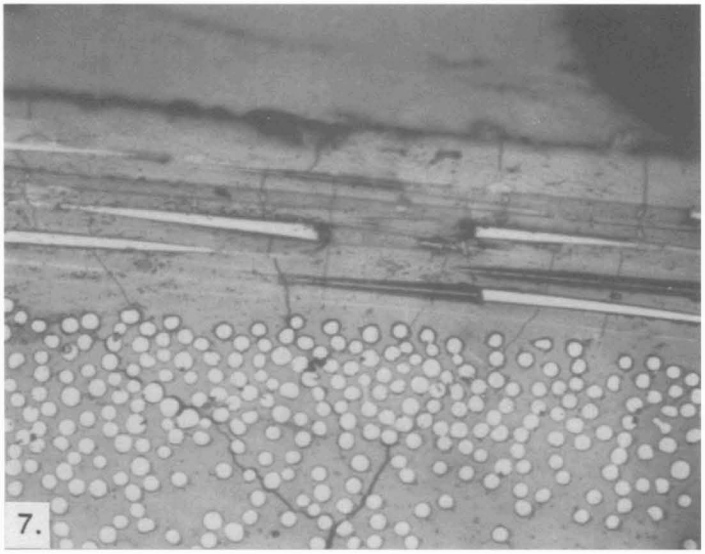

Fig. 7. Interconnection of 0°-ply and 90°-ply macrocracks (formation of "delta" pattern).

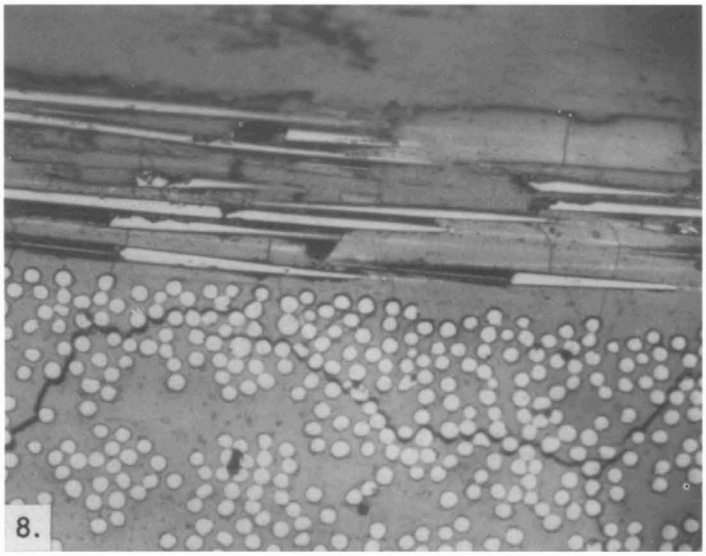

Fig. 8. Longitudinal cracking in 90°-ply.

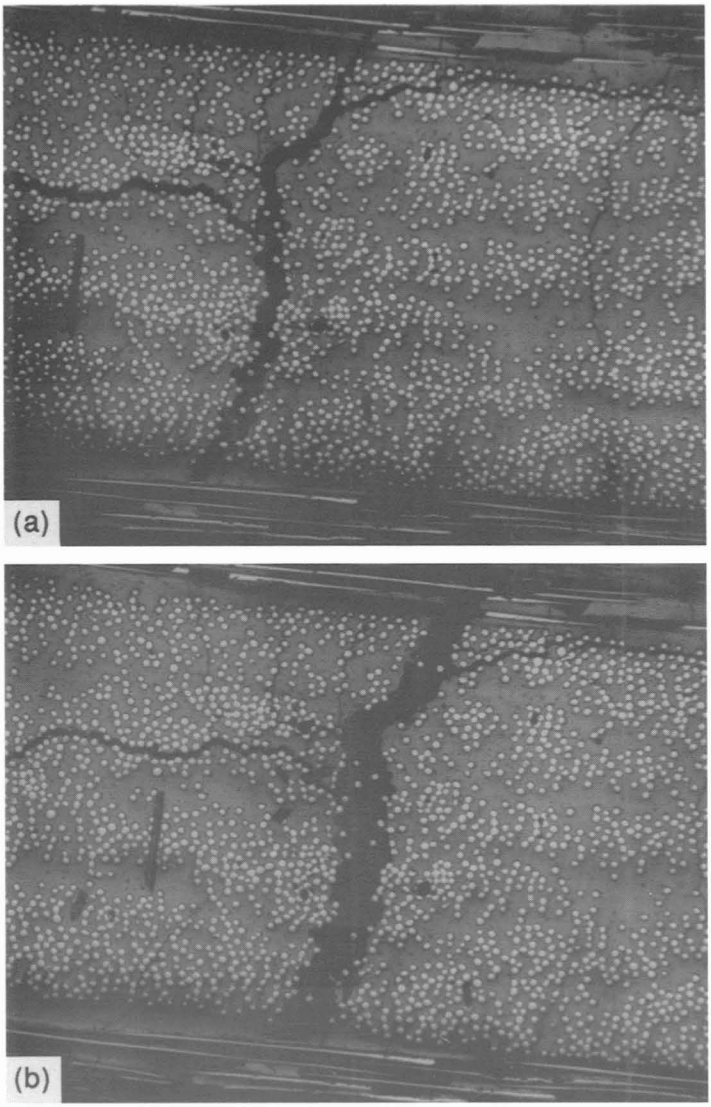

Fig. 9. Final stages of damage consisting of fiber fractures and debonding in 0° layer and crack opening in 90° layer. (a) $\bar{\sigma}_x = 199$ MPa (28.9 ksi), (b) $\bar{\sigma}_x = 210$ MPa (30.4 ksi).

longitudinal stress–strain curve of Fig. 2. Thus, damage in this layer starts near the saturation point of cracking in the 90° layer.

The initial failure in the 0° layer consists of transverse matrix cracks increasing in density with applied stress up to a minimum crack spacing of approx. 120 μm (0.0047 in.) at a stress of 138 MPa (20 ksi) and a strain of 0.37%, as shown in Fig. 6. This is close to the minimum crack spacing observed before in a unidirectional specimen under longitudinal loading and corresponds to eight fiber diameters, Daniel *et al.* (1992).

At this stage of damage development ($\bar{\sigma}_x = 138$ MPa, $\bar{\varepsilon}_x = 0.37\%$) the reduced secant modulus is

$$\bar{E}'_x = 37.3\,\text{GPa}\,(5.4\,\text{Msi}).$$

Assuming no increase in the average axial stress carried by the damaged 90° layer, the following axial moduli and average axial stresses are obtained in each of the two layers:

$$E'_1 = 97\,\text{GPa}\,(14.0\,\text{Msi})$$
$$E'_2 = 7.5\,\text{GPa}\,(1.08\,\text{Msi})$$
$$\sigma_{1x} = 359\,\text{MPa}\,(52\,\text{ksi})$$
$$\sigma_{2x} = 27.6\,\text{MPa}\,(4.0\,\text{ksi}).$$

The further reduction in the layer 2 modulus, while its average axial stress remains constant, is attributed to the increased opening displacements in layer 2 macrocracks, following crack formation and multiplication in layer 1.

One important observation is that the *in situ* reduced axial modulus E'_1 of layer 1 is appreciably higher than the corresponding modulus of the unidirectional material at the same stage of damage development, i.e. saturation of matrix cracks at a strain of $\varepsilon_1 = 0.37\%$ (see Fig. 2). This could be attributed to the fact that large segments of layer 2 remain adhered to layer 1 and bridge the matrix cracks in layer 1, thereby increasing its effective *in situ* stiffness.

At the same point of damage development, there is evidence that extensive fiber–matrix debonding occurs in this layer near and after matrix crack saturation, see Luo *et al.* (1994), Wooh and Daniel (1994). As in the case of the unidirectional material under longitudinal loading, isolated fiber breaks were observed before saturation of transverse matrix cracking in the 0° layers.

Damage interaction between 0° and 90° layers

As the applied stress is increased above 138 MPa (20 ksi), the matrix cracks in the 0° layer begin to propagate into the 90° layer and connect with the macrocracks already developed in that layer. Because of the difference in crack spacings in the two layers, several cracks in the 0° layer connect with each crack in the 90° layer forming a "delta-like" pattern in the 90° layer near the interface (Fig. 7). Each macrocrack in the 90° layer corresponds to five to six transverse cracks in the 0° layer.

With increasing load, axial (in the loading direction) cracks are generated in the 90° layer near the interface with the 0° layer (Fig. 8). These cracks (or delaminations) may be due to high interlaminar shear stresses developed at the tips of the transverse macrocracks in layer 2, and/or high interlaminar normal and shear stresses existing near the edges of crossply laminates (edge effect). Additional transverse cracks also appear in layer 2.

In the final stages of damage development extensive fiber–matrix debonding in layer 1 is accompanied by fiber fractures and sliding. This is manifested by large crack openings in layer 1 and even larger (more than five times larger) crack openings in layer 2 (Fig. 9).

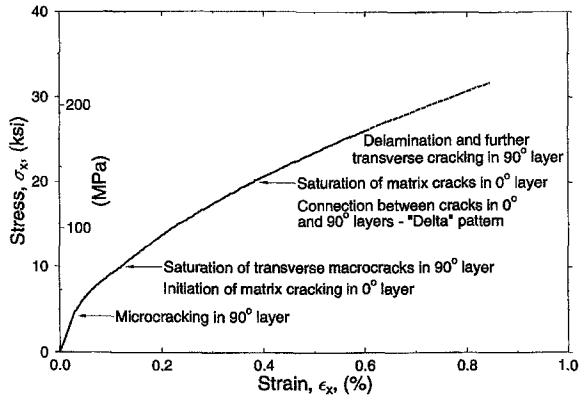

Fig. 10. Stress–strain behavior of $[0/90_2]_s$ laminate with corresponding stages of damage development.

The various failure mechanisms and the entire process of damage evolution are correlated with the macroscopic stress–strain curve of the $[0/90_2]_s$ laminate in Fig. 10. The effects of the various failure mechanisms on stiffness degradation are illustrated.

Ultimate failure occurred at an applied stress of over 220 MPa (32 ksi), which corresponds to an *in situ* longitudinal strength of over 607 MPa (88 ksi) in the 0° layer. This is much higher than any measured longitudinal strength of the unidirectional material and clearly shows the synergistic effect of the 0° and 90° layers of the laminate.

4. ANALYTICAL PREDICTIONS

The formation of transverse macrocracks in the 90° layer of a crossply laminate has been discussed by several investigators, including Reifsnider *et al.* (1983), Talreja (1985), Hashin (1985), Ogin *et al.* (1985), Laws and Dvorak (1988) and Lee and Daniel (1990). The analyses above were aimed primarily at polymer matrix composites, but since they are linear they can be applied to ceramic matrix composites as well. The analytical model described by Lee and Daniel (1990) was used here to explain the observed phenomena. This model was shown to give accurate predictions of stiffness degradation and crack spacing in the 90° layer.

Under axial loading the state of stress in each layer is essentially uniaxial. The first transverse macrocracks in layer 2 occur when the axial (x-axis) stress in that layer reaches the strength of the layer, i.e. the transverse tensile strength, F_{2t}, of the unidirectional material (Fig. 11). As discussed before, the *in situ* transverse strength of the layer is somewhat higher than the value measured by testing an unsupported unidirectional layer. The applied laminate stress $\bar{\sigma}_x$ at crack initiation in layer 2 is

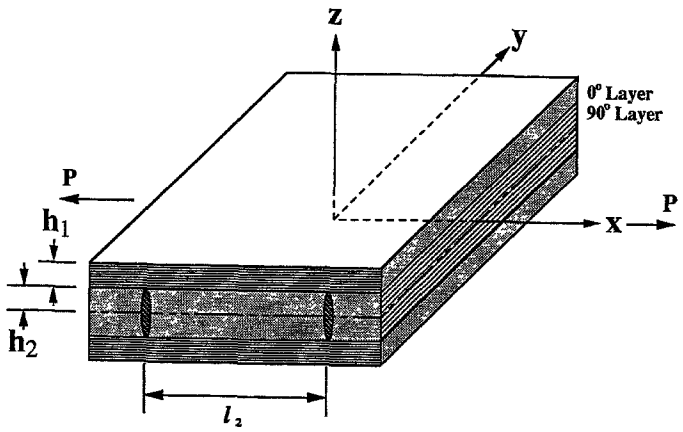

Fig. 11. Element of cracked crossply laminate under axial loading.

$$\bar{\sigma}_x = \frac{\bar{E}_x}{E_2}(F_{2t} - \sigma^r_{2x}), \tag{1}$$

where

$\bar{E}_x = \dfrac{E_1 h_1 + E_2 h_2}{h_1 + h_2}$ = axial modulus of undamaged laminate,

E_1, E_2 = longitudinal and transverse moduli of undamaged unidirectional material, respectively,

F_{2t} = transverse (to the fibers) tensile strength of unidirectional material,

σ^r_{2x} = residual axial stress in 90° layer.

The above residual stress is approximately equal to 7 MPa (1 ksi) for a 1100°C (2000°F) temperature difference between processing and room temperature. Substituting the known material properties and the value $F_{2t} = 38$ MPa (5.5 ksi) for the transverse tensile strength in eqn (1), we obtain a stress of

$$\bar{\sigma}_x = 28.8\,\text{MPa}\,(4.2\,\text{ksi}),$$

which agrees with the experimental observation of initiation of transverse macrocracks in the 90° layer (Fig. 5).

An element of the laminate with the 90° layer cracked under axial loading is shown in Fig. 11. Of particular significance to damage development in the laminate are the stress distributions in the layers and the stiffness reductions. The stress distributions in the layers between two transverse cracks in the 90° layer are given by Lee and Daniel (1990)

$$\sigma_{1x} = \frac{E_1}{\bar{E}_x}\left[1 + \frac{E_2 h_2 \cosh\alpha\left(\frac{l_2}{2} - x\right)}{E_1 h_1 \cosh\alpha\frac{l_2}{2}}\right]\bar{\sigma}_x + \left[1 - \frac{\cosh\alpha\left(\frac{l_2}{2} - x\right)}{\cosh\alpha\frac{l_2}{2}}\right]\sigma^r_{1x} \tag{2}$$

$$\sigma_{2x} = \left[1 - \frac{\cosh\alpha\left(\frac{l_2}{2} - x\right)}{\cosh\alpha\frac{l_2}{2}}\right]\left(\frac{E_2}{\bar{E}_x}\bar{\sigma}_x + \sigma^r_{2x}\right) \tag{3}$$

$$\tau_i = -\alpha h_2\left(\frac{E_2}{\bar{E}_x}\bar{\sigma}_x + \sigma^r_{2x}\right)\frac{\sinh\alpha\left(\frac{l_2}{2} - x\right)}{\cosh\alpha\frac{l_2}{2}}, \tag{4}$$

where σ_{1x}, σ_{2x} = average (through the thickness) axial stresses in 0° and 90° layers, respectively, τ_i = interlaminar shear stress at interface between 0° and 90° layers,

$$\alpha = \left[\frac{(h_1 + h_2)\bar{E}_x}{h_1 h_2 E_1 E_2} \cdot \frac{3G_{12}G_{23}}{h_1 G_{23} + h_2 G_{12}}\right]^{1/2}, \tag{5}$$

G_{12}, G_{23} = in-plane and out-of-plane shear moduli of undamaged unidirectional material, σ^r_{1x} = axial residual stress in 0° layer (calculated as -13 MPa), l_2 = crack spacing in 90° layer.

This crack spacing decreases with load up to a minimum characteristic value. Experimentally, a minimum crack spacing of 0.65 mm (0.0255 in.) was observed at an applied stress of $\bar{\sigma}_x = 69$ MPa (10 ksi), as mentioned before. The predicted crack spacing at this stress can be obtained by setting $\bar{\sigma}_x = 69$ MPa (10 ksi), $\sigma_{2x} = F_{2t} = 38$ MPa (5.5 ksi) and $x = l_2/2$ (midpoint between cracks) in eqn (3). Then, from eqn (3) we obtain

$$l_2 = \frac{2}{\alpha}\cosh^{-1}\eta \tag{6}$$

where

$$\eta = \left[1 - \frac{F_{2t}}{\frac{E_2}{\bar{E}_x}\bar{\sigma}_x + \sigma^r_{2x}}\right]^{-1}.$$

For the numerical values above we obtain

$$(l_2)_{\min} = 0.68\,\text{mm}\,(0.027\,\text{in.}).$$

Expressions for the reduced axial stiffness E'_2 of the 90° layer and $\bar{E}'_x$ of the laminate are given as a function of crack spacing as follows, Lee and Daniel (1990):

$$\bar{E}'_2 = \frac{(1-\beta)(E_2\bar{\sigma}_x + \bar{E}_x\sigma^r_{2x})}{\left(1 + \frac{E_2 h_2}{E_1 h_1}\beta\right)\bar{\sigma}_x + \frac{\bar{E}_x}{E_1}(1-\beta)\sigma^r_{1x}} \tag{7}$$

and

$$\bar{E}'_x = \bar{E}_x\left[1 + \frac{E_2 h_2}{E_1 h_1}\beta + \frac{\sigma^r_{1x}}{\bar{\sigma}_x}\frac{\bar{E}_x}{E_1}(1-\beta)\right]^{-1}, \tag{8}$$

where

$$\beta = \frac{2}{\alpha l_2}\tanh\left(\frac{\alpha l_2}{2}\right).$$

At the applied stress level of 69 MPa (10 ksi), where transverse crack saturation was noticed, but before any substantial damage occurred in the 0° layer, the 90° layer and laminate moduli are calculated as

$$E'_2 = 19\,\text{GPa}\,(2.8\,\text{Msi})$$
$$\bar{E}'_x = 55\,\text{GPa}\,(8.0\,\text{Msi}),$$

which are in good agreement with the experimental values of $E'_2 = 22.8$ GPa (3.3 Msi) and $\bar{E}'_x = 58$ GPa (8.3 Msi) mentioned before.

The average stress carried by the 0° layer then, is

$$\sigma_{1x} \cong \sigma^r_{1x} + \frac{E_1}{\bar{E}'_x}\bar{\sigma}_x = 146\,\text{MPa}\,(21.1\,\text{ksi}).$$

The stress necessary to initiate transverse matrix cracking in the 0° layer is

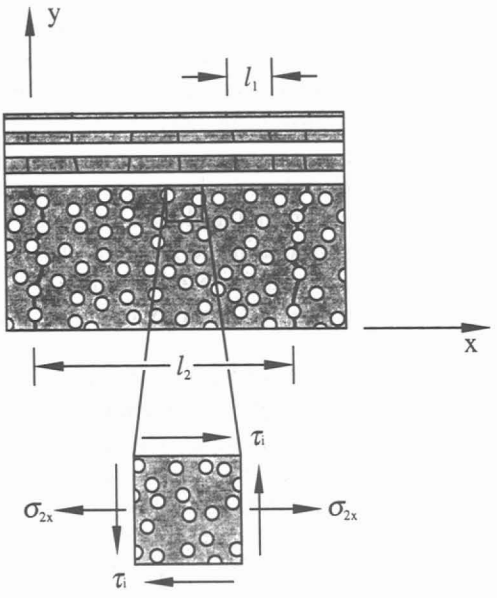

$$l_2 \cong 6l_1$$

Fig. 12. Element of laminate with both layers cracked up to their saturation levels.

$$\sigma_{1x} = \frac{E_1}{E_m}(F_{mt} - \sigma^r_{mx}) - \sigma^r_{1x}$$

where E_m = matrix modulus, F_{mt} = matrix tensile strength, σ^r_{mx} = axial micro-residual stress in matrix of 0° layer.

Neglecting the counteracting residual stresses, tensile micro-residual stress σ^r_{mx} and compressive macro-residual stress σ^r_{1x}, we obtain the value

$$\sigma_{1x} \cong 154 \text{ MPa } (22.3 \text{ ksi}).$$

This shows that crack initiation takes place in the 0° layer at a slightly higher load level than that at which crack saturation occurs in the 90° layer. This also corresponds to the observed proportional limit of the longitudinal stress–strain curve (Fig. 2).

Cracking continues in the 0° layer up to a saturation crack density where $(l_1)_{min} = 0.120$ mm (0.0047 in.), which is one-sixth to one-fifth of $(l_2)_{min}$. An element of the laminate with both layers cracked up to their saturation levels is shown in Fig. 12. A subelement of the 90° layer at the interface with the 0° layer is subjected primarily to the normal axial stress σ_{2x} and interlaminar shear stress τ_i. These stresses result in a tensile principal stress at an angle that would explain the formation of branch cracks in the observed "delta" pattern.

5. SUMMARY AND CONCLUSIONS

The behavior of crossply ceramic-matrix composites under axial tensile loading was studied. The material investigated was SiC/CAS, calcium aluminosilicate glass-ceramic reinforced with silicon carbide (Nicalon) fibers. Specimens were loaded under the microscope and the various failure mechanisms, their sequence, interaction and overall damage development were observed in real time and recorded.

The first stage of damage development consists of microcracks in the 90° layer, which then develop into transverse macrocracks. These macrocracks increase in density up to a saturation limit, with a minimum crack spacing approximately equal to the 90° layer thickness. Thereafter, transverse matrix cracks are generated in the 0° layer. These cracks

also increase in density up to a minimum crack spacing of approximately eight fiber diameters. In the third stage of damage development there is an interconnection of the two sets of cracks. Several of the denser 0° layer cracks connect with each of the 90° layer cracks in a delta-like pattern. This is finally followed by delaminations and additional cracking in the 90° layer prior to ultimate failure.

Damage development was correlated with the macroscopic stress–strain response of the unidirectional material under longitudinal and transverse loading and of the crossply laminate. It was noticed that first-ply failure in the 90° layer occurs at a higher layer stress than the transverse tensile strength of the unidirectional material. This may be attributed to the constraining effects of the 0° layer which tend to increase the *in situ* transverse tensile strength of the 90° layer.

Following crack saturation in the 90° layer, cracking initiated and increased in the 0° layers at approximately the same strain levels where similar cracking was observed in the unidirectional material under longitudinal loading. However, the 0° layer stresses at the various stages of damage development, were higher than corresponding stress levels in the 0° unidirectional specimen for the same damage. This was explained as a stiffening or strengthening effect of the 0° layers caused by the attached 90° layer. Ultimate failure of the laminate clearly showed the synergistic effects of the 0° and 90° layers of the laminate.

Damage development in the 90° layer was compared with analytical predictions. A model developed previously for crossply graphite/epoxy composites was used to predict cracking in the 90° layer and stiffness degradation, both in the 90° layer and in the overall laminate. The predictions were in very good agreement with experimental observations.

It was shown that the overall damage development is characterized by different scales at different stages. The relevant scales are fiber diameter and fiber spacing for failure initiation in the 90° layer; layer thickness for damage saturation in the 90° layer; and fiber diameter for matrix cracking in the 0° layer. Finally, there is a scale crossing phenomenon in the interaction between the damage in the 90° and 0° layers.

Acknowledgement—The work described here was sponsored by the Air Force Office of Scientific Research (AFOSR). We are grateful to Dr Walter F. Jones of the AFOSR for his encouragement and cooperation; to Mr David Larsen of Corning Glass Works for supplying material; to Mrs Yolande Mallian for typing the manuscript; and Mr J. J. Luo and Dr C. L. Tsai for their assistance with the figures.

REFERENCES

Achenbach, J. D. and Zhu, H. (1990). Effect of interphases on micro and macromechanical behavior of hexagonal-array fiber composites. *J. Appl. Mech.* **57,** 956–963.

Aveston, J. and Kelly, A. (1973). Theory of multiple fracture of fibrous composites. *J. Mater. Sci.* **8,** 352–362.

Aveston, J., Cooper, G. A. and Kelly, A. (1971). The properties of fibre composites. *Conf. Proc., National Physical Laboratory*, pp. 15–26. IPC Science and Technology Press, Surrey, U.K.

Benveniste, Y. (1985). The effective mechanical behavior of composite materials with imperfect contact between the constituents. *Mech. Mater.* **4,** 197–208.

Brennan, J. J. and Prewo, K. M. (1982). Silicon carbide fibre reinforced glass-ceramic matrix composites exhibiting high strength and toughness. *J. Mater. Sci.* **17,** 2371–2383.

Budiansky, B., Hutchinson, J. W. and Evans, A. G. (1986). Matrix fracture in fiber-reinforced ceramics. *J. Mech. Phys. Solids* **34** (13), 167–189.

Charalambides, P. G. (1991). Steady-state mechanics of delamination cracking in laminated ceramic-matrix composites. *J. Am. Ceram. Soc.* **74** (12), 3066–80.

Charalambides, P. G. and Evans, A. G. (1989). Debonding properties of residually stressed brittle-matrix composites. *J. Am. Ceram. Soc.* **72,** 746–53.

Daniel, I. M., Anastassopoulos, G. and Lee, J.-W. (1989a). Failure mechanisms in ceramic-matrix composites. *Proc. SEM Spring Conf. Experimental Mechanics*, 29 May–1 June, 1989, 832–838.

Daniel, I. M., Anastassopoulos, G. and Lee, J.-W. (1989b). Experimental micromechanics of brittle-matrix composites. *Micromechanics: Experimental Techniques*, Vol. AMD **102,** pp. 133–146. ASME Winter Annual Meeting, San Francisco, CA.

Daniel, I. M., Anastassopoulos, G. and Lee, J.-W. (1992). Failure mechanisms and interfacial shear strength in brittle-matrix composites. *Advances in Experimental Mechanics and Biomimetics*, Vol. AD 29/AMD 146, (Edited by W. F. Jones and J. M. Whitney), pp. 57–69. ASME.

Daniel I. M., Lee, J.-W. and Anastassopoulos, G. (1993). The behavior of ceramic matrix fiber composites under longitudinal loading. *Compos. Sci. Technol.* **46,** 105–113.

Daniel, I. M., Lee, J.-W. and Yaniv, G. (1988). Damage development and property degradation of composite materials. In *Mechanics of Composite Materials* (Edited by G. J. Dvorak and N. Laws), Vol. **AMD92,** 149–160. ASME.

Hashin, Z. (1983). Analysis of composite materials—a survey. *J. Appl. Mech.* **50,** 481–505.

Hashin, Z. (1985). Analysis of cracked laminates; a variational approach. *Mech. Mater.* **4,** 121–136.
Hsueh, C.-H. (1988). Analytical evaluation of interfacial shear strength for fiber-reinforced ceramic composites. *J. Am. Ceram. Soc.* **71,** 490–493.
Hutchinson, J. W. and Jenson, H. M. (1990). Models of fiber debonding and pullout in brittle composites with friction. *Mech. Mater.* **9,** 139–163.
Larsen, D. C. and Adams, J. (1989). Corning glass works. Private communication.
Laws, N. and Dvorak, G. J. (1988). Progressive transverse cracking in composite laminates. *J. Compos. Mater.* **22,** 900–916.
Lee, J.-W and Daniel, I. M. (1990). Progressive transverse cracking of crossply composite laminates. *J. Compos. Mater.* **24,** 1225–1243.
Lee, J.-W. and Daniel, I. M. (1992). Deformation and failure of longitudinally loaded brittle-matrix composites. In *Composite Materials: Testing and Design*, Vol. ASTM, STP 1120 (Edited by Glenn C. Grimes), pp. 204–221. American Society for Testing and Materials, Philadelphia.
Luo, J.-J., Wooh, S.-C. and Daniel, I. M. (1994). Acoustic emission study of failure mechanisms in ceramic matrix composite under longitudinal tensile loading. *Review of Progress in QNDE*, Vol. **13** (Edited by D. O. Thompson and D. E. Chimenti), pp. 469–476. Plenum Press, New York.
Mall, S. and Kim, R. Y. (1992). Failure mechanisms in laminates of silicon carbide calcium–aluminosilicate ceramic composite. *Composites* **23** (4), 215–222.
Marshall, D. B. and Evans, A. G. (1985). Failure mechanisms in ceramic-fiber/ceramic-matrix composites. *J. Am. Ceram. Soc.* **68,** 225–231.
Marshall, D. B. and Evans, A. G. (1988). Failure mechanisms in ceramic-fiber/ceramic-matrix composites. *Ceram. Engng Sci. Proc.* **9** (7–8), 853–860.
Marshall, D. B., Cox, B. N. and Evans, A. G. (1985). The mechanics of matrix cracking in brittle-matrix fiber composites. *Acta Metall.* **33** (11), 2013–2021.
McCartney, L. N. (1989). New theoretical model of stress transfer between fibre and matrix in a unidirectionally fibre-reinforced composite. *Proc. R. Soc. Lond. Ser.* **A425,** 215–244.
Ogin, S. L., Smith, P. A. and Beaumont, P. W. R. (1985). Matrix cracking and stiffness reduction during the fatigue of a [0/90] GFRP laminate. *Compos. Sci. Technol.* **22,** 23–31.
Prewo, K. M. and Brennan, J. J. (1982). Silicon carbide yarn reinforced glass matrix composites. *J. Mater. Sci.* **17,** 1201–1206.
Reifsnider, K. L., Henneke, E. G., Stinchcomb, W. W. and Duke, J. C. (1983). Damage mechanisms and NDE of composite laminates. *Mechanics of Composite Materials; Recent Advances (Proc. IUTAM Symp. Mechanics of Composite Materials)* (Edited by Z. Hashin and C. T. Herakovich), pp. 399–420. Pergamon Press, New York.
Sbaizero, O. and Evans, A. G. (1986). Tensile and shear properties of laminated ceramic matrix composites. *J. Am. Ceram. Soc.* **69**(6), 481–486.
Sbaizero, O., Charalambides, P. G. and Evans, A. G. (1990). Delamination cracking in a laminated ceramic-matrix composite. *J. Am. Ceram. Soc.* **73** (7), 1936–1940.
Stang, H. and Shah, S. P. (1986). Failure of fiber-reinforced composites by pull-out fracture. *J. Mater. Sci.* **21,** 953–957.
Talreja, R. (1985). Transverse cracking and stiffness reduction in composite laminates. *J. Compos. Mater.* **19,** 355–375.
Weitsman, Y. and Zhu, H. (1993). Multi-fracture of ceramic composites. *J. Mech. Phys. Solids* **41** (2), 351–388.
Wooh, S.-C. and Daniel, I. M. (1994). Real-time ultrasonic monitoring of fiber-matrix debonding in ceramic matrix composite. *Mech. Mater.* **17,** 379–388.
Zhu, H. and Achenbach, J. D. (1991). Radial matrix cracking and interphase failure in transversely loaded fiber composites. *Mech. Mater.* **11,** 347–356.
Zok, F. W. and Spearing, S. M. (1992). Matrix crack spacing in brittle matrix composites. *Acta Metall. Mater.* **40** (8), 2033–2043.